Non-isothermal crystallization kinetics of some aventurine decorative glaze

**C. Păcurariu · R. I. Lazău · I. Lazău ·
D. Tiţa · A. Dumitrel**

Abstract Non-isothermal crystallization of hematite in an aventurine glaze was investigated using DTA technique. The apparent activation energy as a function of the crystallized fraction was evaluated by the Kissinger–Akahira–Sunose (KAS), Ozawa–Flynn–Wall (OFW), Starink, Tang, and Vyazovkin isoconversional methods. The apparent activation energy of the hematite crystallization in the studied aventurine glaze ranges with the crystallization fraction between 150 and 180 kJ mol^{-1}. The Avrami exponent values, calculated by Ozawa method confirm the complex mechanism of the crystallization process.

Keywords Crystallization kinetics · Isoconversional methods · Aventurine glazes

Introduction

The crystallized aventurine glazes are highly alkaline glazes with golden scintillations due to the presence of iron, chromium, uranium, etc., oxides [1]. From the aventurine glazes, the most representative are those with iron oxide content ranging between 10 and 30%. The decorative effect of these iron-aventurine glazes is influenced by the proportion and size of the hexagonal hematite crystals, which emerge inside the glaze layer and develop a strong shine [2, 3]. The color of these glazes range from light to dark reddish-brown depending on the iron oxide content.

The hematite crystallization in the aventurine glazes is due to the oversaturation of the melting with Fe^{3+} cations during the cooling process, making possible the hematite (α-Fe_2O_3) crystals separation [2, 3].This crystallization mechanism is strongly influenced by the oxide composition of the melt (the ratio between the acid oxides and the base oxides) and especially by the melt viscosity, which determine hematite proportion and the size of the developing crystals.

This article focuses on the kinetics study of the hematite crystallization in an aventurine glaze. The apparent activation energy, as a function of the extent of conversion, was evaluated by the Kissinger–Akahira–Sunose (KAS), Ozawa–Flynn–Wall (OFW), Starink, Tang, and Vyazovkin isoconversional methods. The Avrami exponent "n" of the crystallization process was also evaluated using the Ozawa method.

Experimental

Sample preparation

The oxide composition of the frit (A4) used for obtaining the aventurine glaze was: 41% SiO_2, 26% B_2O_3, 11% Na_2O, 6% PbO, and 16% Fe_2O_3 (mass%). The mixture of raw materials (borax, quartz, litharge, boric acid) was melted at 1260 °C for 1 h in an electric furnace. Black, granular frit resulted after pouring the melt in cold water. At the further thermal treatment of the frit, golden crystals of hematite (α-Fe_2O_3) separated from the vitreous matrix. Part of the hematite remains in the yellow-orange to reddish-brown vitreous matrix.

C. Păcurariu (✉) · R. I. Lazău · I. Lazău · A. Dumitrel
Faculty of Industrial Chemistry and Environmental Engineering,
"Politehnica" University of Timişoara, P-ţa Victoriei No. 2,
300006 Timisoara, Romania
e-mail: cornelia.pacurariu@chim.upt.ro

D. Tiţa
Faculty of Pharmacy, University of Medicine and Pharmacy
"Victor Babeş", P-ţa E. Murgu no.2, Timisoara, Romania

The obtained frit was then used for preparing a ceramic glaze with 95% frit and 5% kaolin homogenized in a Pulverisette ball mill for 10 min, at a relative humidity of 23% (100 g solid materials and 30 mL water).

Characterization methods

The hematite crystallization in the prepared frit (A4) was investigated using a NETZSCH-STA 449C TG/DTA instrument in nitrogen atmosphere at a flow rate of 20 mL min^{-1}. For the kinetics study of the hematite crystallization, the non-isothermal DTA curves were recorded in a temperature range starting from ambient temperature up to 800 °C, at heating rates of 5, 8, 10, 12, 14, 16 °C min^{-1}, using platinum crucibles. The samples mass was $m = 211$ mg.

The hematite presence in the sample was confirmed by XRD analysis using a DRON 3 diffractometer with CuKα radiation.

The hematite crystallization degree and the crystals shape and size were analyzed by optical microscopy in reflected light using a Guangzhou L 2020A microscope with digital camera.

Theoretical

Kinetics of solid-state reactions is usually described by the equation:

$$g(\alpha) = \frac{A}{\beta} \int_0^T e^{-\frac{E}{RT}} dT = \frac{AE}{\beta R} \int_x^\infty \frac{e^{-x}}{x^2} dx = \frac{AE}{\beta R} p(x) \qquad (1)$$

where $x = E/RT$ and $p(x)$ is termed *the temperature integral* and has no analytical solution.

Many methods have been proposed [4–11] for estimating the activation energy. The most reliable methods are considered those which involve the determination of the temperature $T_\alpha(\beta)$ at which a certain conversion (α) corresponding to a certain heating rate (β) reached [5]. These methods are called isoconversional methods and allow the activation energy to be determined as a function of the extent of conversion helping at the same time to reveal the complexity of the reaction kinetics [4, 12, 13]

The isoconversional integral methods depend on the temperature integral approximation and require data on $T_\alpha(\beta)$. These methods can be classified into two groups: linear and non-linear integral isoconversional methods [14].

Linear integral isoconversional methods

Many approximations of the temperature integral $p(x)$ have been suggested in the literature and as a consequence, many more or less accurate methods appeared for the activation energy analysis [1, 5, 7, 9, 15]. All these methods involve the plot of a logarithmic function (which depends on the approximation for the temperature integral used) versus $1/T_\alpha$. The general equation is:

$$\ln \frac{\beta}{T_\alpha^\kappa} = -A \frac{E_\alpha}{RT_\alpha} + C \qquad (2)$$

where κ is a constant depending on the approximation of the temperature integral employed, A and C are constants and the subscript α designates values related to a given extent of conversion.

Four of the linear integral isoconversional methods, considered in the literature the most accurate, were used in this article.

Kissinger–Akahira–Sunose method

The Kissinger–Akahira–Sunose (KAS) method is based on the approximation $p(x) \cong e^{-x}/x^2$ $(20 < x < 50)$ for the temperature integral [5, 7, 10, 16]. In this case, at constant conversion α, the general linear equation (2) leads to Eq. 3 ($\kappa = 2$):

$$\ln \frac{\beta}{T_\alpha^2} = -\frac{E_\alpha}{RT_\alpha} + C \qquad (3)$$

Ozawa–Flynn–Wall method

The Ozawa–Flynn–Wall (OFW) method is based on Doyle's approximation for the temperature integral, $p(x) \cong e^{-1.052x - 5.330}$ $(20 < x < 60)$ [5, 7, 10, 16, 17]. For this method, $\kappa = 0$ and for constant conversion α, the general linear equation (2) becomes:

$$\ln \beta = -1.052 \frac{E_\alpha}{RT_\alpha} + C \qquad (4)$$

Starink method

The approximation suggested by Starink [5, 7] for the temperature integral is $p(x) \cong e^{\frac{-1.0008x - 0.312}{x^{1.92}}}$. In this case, $\kappa = 1.92$ and at constant conversion α, the general linear equation (2) becomes:

$$\ln \frac{\beta}{T_\alpha^{1.92}} = -1.0008 \frac{E_\alpha}{RT_\alpha} + C \qquad (5)$$

Tang method

The approximation proposed by Tang [18, 19] for the temperature integral is: $-\ln p(x) = 0.37773896 + 1.894661 \ln x + 1.00145033x$. For this method, ($\kappa = 1.894661$) and at constant conversion α, the general linear equation (2) becomes:

$$\ln \frac{\beta}{T_\alpha^{1.894661}} = -1.00145033 \frac{E_\alpha}{RT_\alpha} + C \tag{6}$$

Non-linear integral isoconversional method

To increase the accuracy of activation energy assessment, Vyazovkin [13, 20, 21] developed a non-linear isoconversional method. For a set of n experiments carried out at different heating rates, the activation energy can be determined at any value of α by finding the value of E_α, which minimizes the function:

$$\Omega = \sum_{i=1}^{n} \sum_{\substack{j=1 \\ j \neq i}}^{n} \frac{I(E_\alpha, T_{\alpha i})\beta_j}{I(E_\alpha, T_{\alpha j})\beta_i} \tag{7}$$

where:

$$I(E_\alpha, T_{\alpha i}) = \int_0^{T_{\alpha i}} \exp\left(\frac{-E_\alpha}{RT}\right) dT \tag{8}$$

The minimization procedure is repeated for each value of α, to find the dependence of the activation energy on the extent of conversion. In our article, the integral (Eq. 8) was evaluated using three different approximations (Eqs. 9–11):Gorbachev [22, 23]:

$$I(E_\alpha, T_{\alpha i}) = \int_0^{T_{\alpha i}} \exp\left(\frac{-E_\alpha}{RT}\right) dT = \frac{RT_{\alpha i}^2}{E_\alpha + 2RT_{\alpha i}} \exp\left(-\frac{E_\alpha}{RT_{\alpha i}}\right) \tag{9}$$

Agrawal and Sivasubramanian (AS) [22, 23]:

$$I(E_\alpha, T_{\alpha i}) = \int_0^{T_{\alpha i}} \exp\left(\frac{-E_\alpha}{RT}\right) dT$$
$$= \frac{RT_{\alpha i}^2}{E_\alpha} \left[\frac{1 - \frac{2RT_{\alpha i}}{E_\alpha}}{1 - 5\left(\frac{RT_{\alpha i}}{E_\alpha}\right)^2} \right] \exp\left(-\frac{E_\alpha}{RT_{\alpha i}}\right) \tag{10}$$

Cai et al. [24]:

$$I(E_\alpha, T_{\alpha i}) = \int_0^{T_{\alpha i}} \exp\left(\frac{-E_\alpha}{RT}\right) dT$$
$$= \frac{RT_{\alpha i}^2}{E_\alpha} \left[\frac{E_\alpha/RT_{\alpha i} + 0.66691}{E_\alpha/RT_{\alpha i} + 2.64943} \right] \exp\left(-\frac{E_\alpha}{RT_{\alpha i}}\right) \tag{11}$$

The crystallized fraction $\alpha(T)$ was determined from the DTA curves using Eq. 12:

$$\alpha(T) = \frac{A_{(T)}}{A_{(Total)}} \tag{12}$$

where $\alpha(T)$ is the crystallized fraction at the temperature T, $A_{(T)}$ is the area at the temperature interval ΔT, and $A_{(Total)}$ is the total area of the crystallization peak.

In order to obtain information about the crystallization mechanism, the Avrami exponent, n, was evaluated using the equation suggested by Ozawa [25]:

$$\log[-\ln(1 - \alpha)] = \log \chi(T) - n \log \beta \tag{13}$$

where $\chi(T)$ is a constant.

The Avrami exponent n results from the slope of the plot of $\log[-\ln(1 - \alpha)]$ versus $\log \beta$ at a given temperature.

Results and discussion

Figure 1 shows the DTA crystallization curves of frit A4, recorded at six different heating temperatures.

The crystallized fraction α, was evaluated from the DTA curves using Eq. 12. Figure 2 shows the variation of the crystallized fraction as a function of temperature, for all the heating rates used.

Kissinger–Akahira–Sunose method

The activation energies of the crystallization process at different crystallized fractions were calculated using Eq. 3). For constant crystallized fraction, the value of E_α resulted from the slope of the linear fitted function of $\ln(\beta/T_\alpha^2)$ versus T_α^{-1}. The KAS plots are shown in Fig. 3 for different crystallized fraction.

Ozawa–Flynn–Wall method

Using the OFW method, the activation energies for the crystallization process were calculated from the slope of the linear fitted function of $\ln \beta$ versus T_α^{-1} (Eq. 4), for
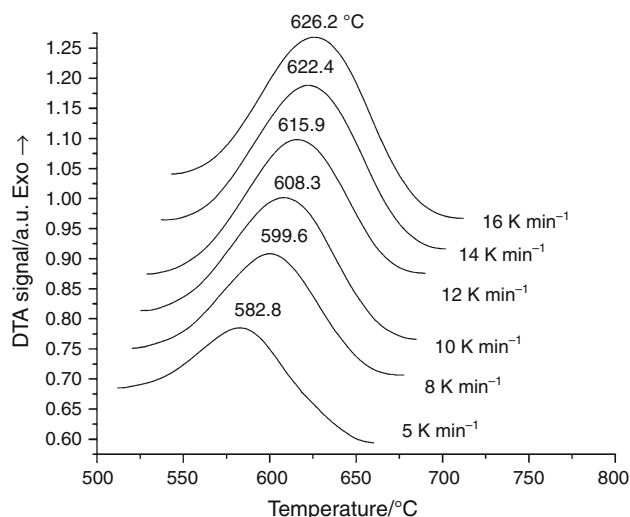

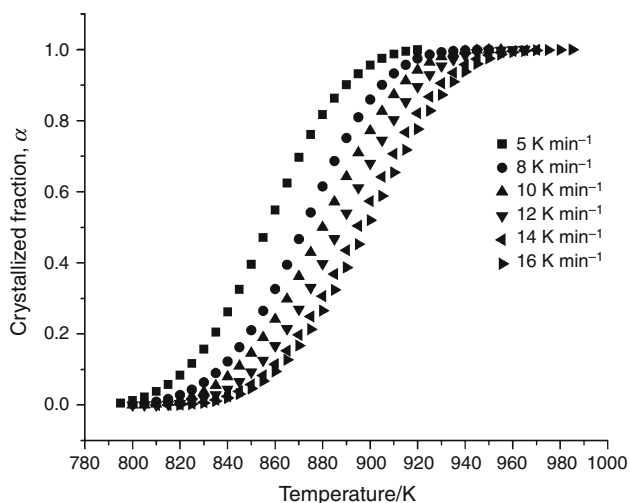**Fig. 1** DTA crystallization curves of frit A4, for different heating rates

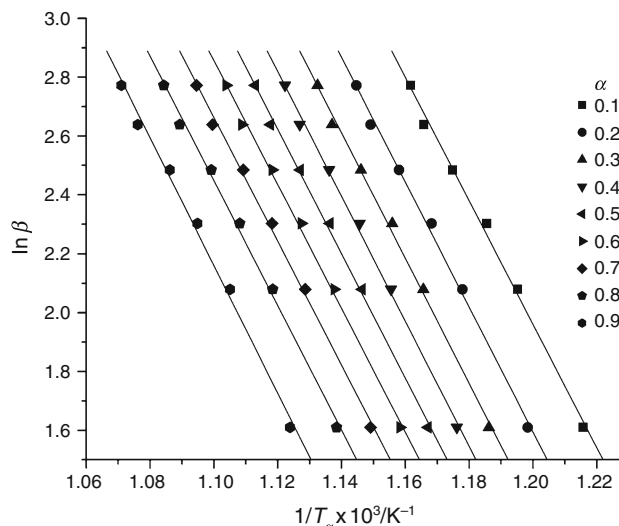**Fig. 2** Crystallized fraction α versus temperature at different heating rates

Fig. 4 Plots of In β versus T_α^{-1} at different crystallized fractions
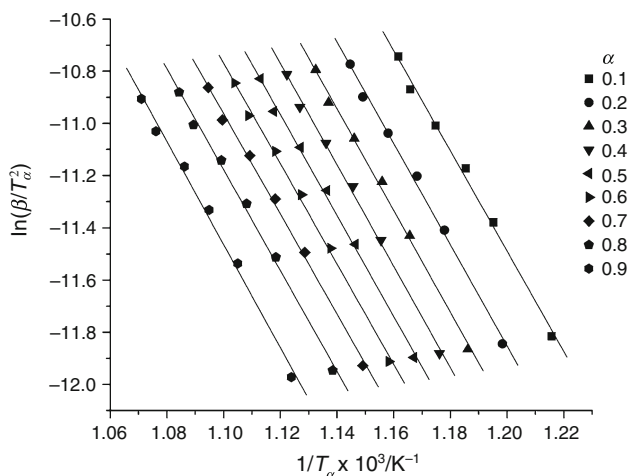

Fig. 3 Plots of $\ln(\beta/T_\alpha^2)$ versus T_α^{-1} at different crystallized fractions
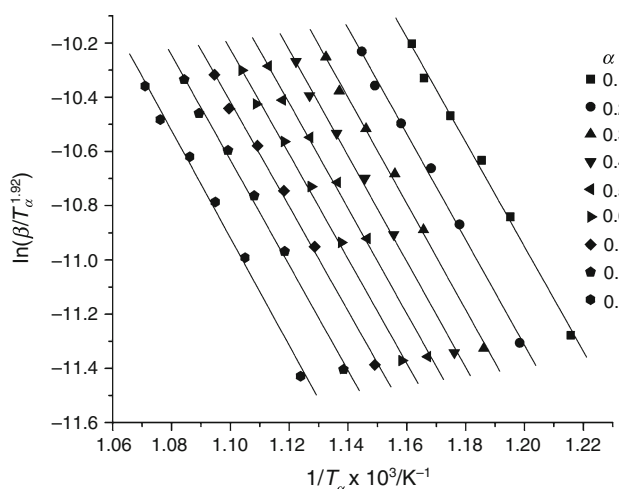

Fig. 5 Plots of $\ln(\beta/T_\alpha^{1.92})$ versus T_α^{-1} at different crystallized fractions

different crystallized fractions. The OFW plots are shown in Fig. 4 for different crystallized fractions.

Starink method

Using the Starink method, the values of E_α was calculated from the slope of the linear fitted function of $\ln(\beta/T_\alpha^{1.92})$ versus T_α^{-1} (Eq. 5) for constant crystallized fraction. The Starink plots for different crystallized fractions are shown in Fig. 5.

Tang method

The activation energies of the crystallization process at different crystallized fractions were calculated using Eq. 6. For constant crystallized fraction, the value of E_α resulted

from the slope of the linear fitted function of $\ln(\beta/T_\alpha^{1.894661})$ versus T_α^{-1}. The Tang plots for different crystallized fractions are shown in Fig. 6.

Figure 7 shows the activation energy evaluated by Vyazovkin equation (Eq. 7) as a function of crystallized fraction. For comparison, there are presented the E_α values evaluated with Gorbachev (Eq. 9), AS (Eq. 10), respectively, Cai (Eq. 11) approximations.

Comparing the values of the activation energies evaluated by the three presented approximations one may notice they are very close. The values of the activation energies are almost identical for Gorbachev and AS and slightly lower for Cai approximation.

Figure 8 shows comparatively, the variation of the activation energies evaluated by KAS, OFW, Starink,
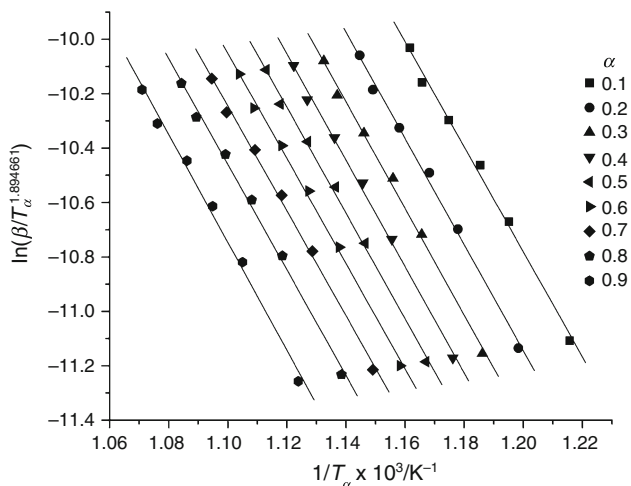
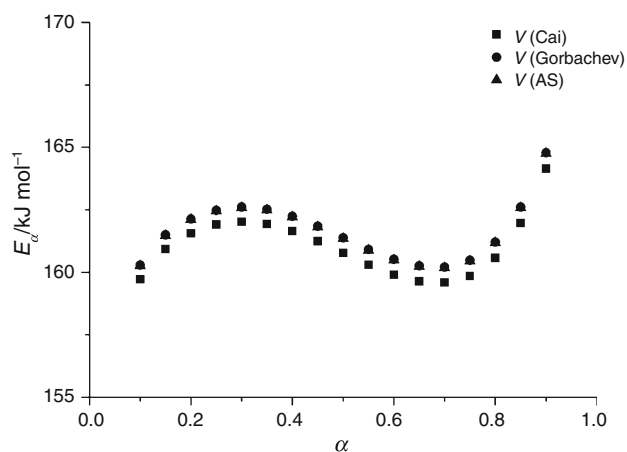**Fig. 6** Plots of $\ln(\beta/T_\alpha^{1.894661})$ versus T_α^{-1} at different crystallized fractions

Fig. 7 Variation of E_α as a function of α, evaluated by Vyazovkin method, using Gorbachev, AS, and Cai approximations
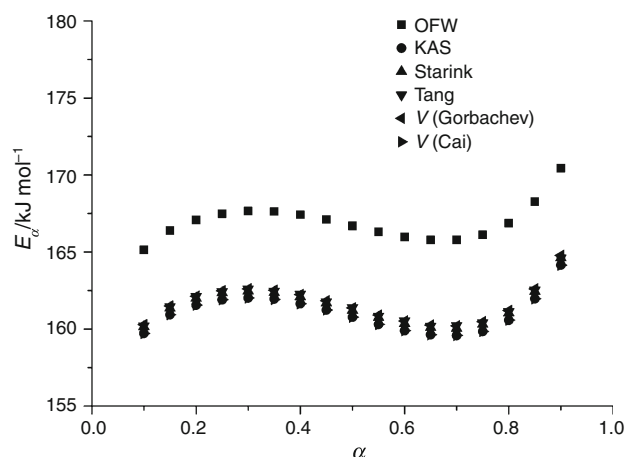

Fig. 8 Variation of E_α evaluated by different isoconversional methods as a function of α

Tang, and Vyazovkin (Gorbachev and Cai approximations) methods as a function of crystallized fraction.

On the basis of obtained results, the following observations have been made:

– The activation energies evaluated by KAS, Starink, Tang, and Vyazovkin methods show very close values in the entire range of the crystallized fraction. These results are in agreement with the literature data regarding the accuracy provided by these methods [5, 23, 24].
– The activation energies evaluated by OFW method show a little higher values compared with the other methods investigated, in the entire range of the crystallized fraction.
– The activation energies evaluated by Vyazovkin method (using Cai approximation) show only slightly lower values compared with KAS, Starink, Tang, and Vyazovkin (using Gorbachev and AS approximation) methods, in the entire range of the crystallized fraction.
– The activation energy varies with the crystallized fraction regardless of the method used. This behavior confirms the complex mechanism of the crystallization process. Therefore, the calculated activation energies are apparent values, depending on the activation energies of the elementary processes (nucleation and growth).

Figure 9 shows the plots of $\log[-\ln(1-\alpha)]$ as a function of $\log \beta$ at different temperatures.

Table 1 summarizes the values of Avrami exponent, calculated from Eq. 13 ($1\% < \alpha < 99\%$).

Table 1 shows that n values range approximately between 1.23 ± 0.06 and 1.93 ± 0.12, the average value being around 1.5.
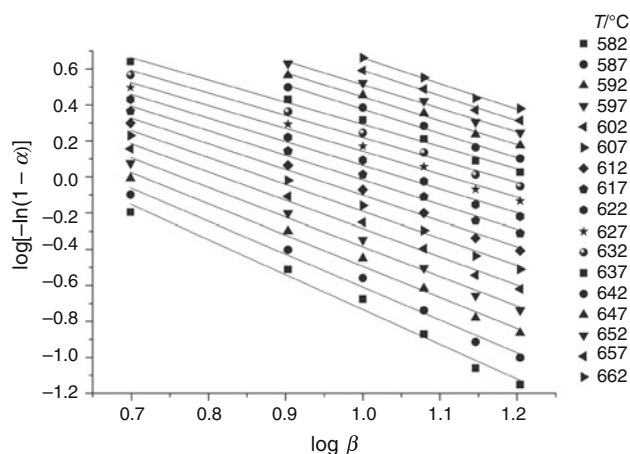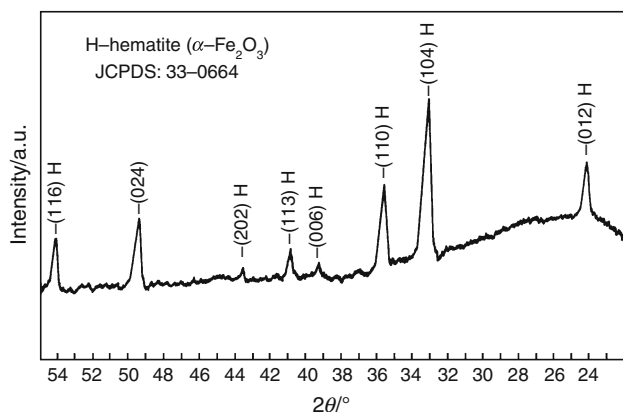

Fig. 9 Plots of $\log[-\ln(1-\alpha)]$ as a function of $\log \beta$ at different temperatures

Table 1 Avrami exponents n and the correlation coefficients r^2 at different temperatures
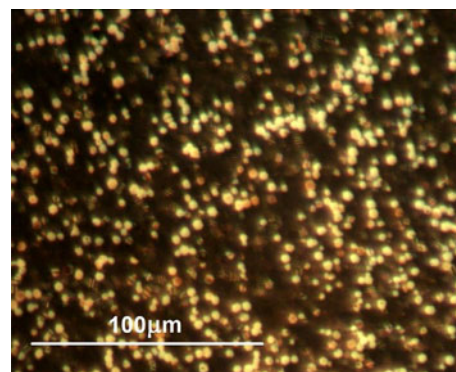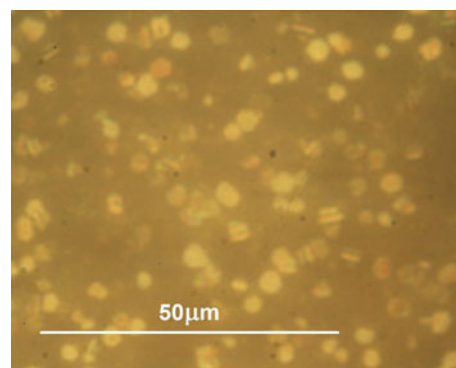
Temperature $T/°C$	n	r^2
582	1.93 ± 0.12	0.9819
587	1.82 ± 0.10	0.9846
592	1.72 ± 0.09	0.9866
597	1.64 ± 0.08	0.9877
602	1.56 ± 0.07	0.9881
607	1.49 ± 0.07	0.9878
612	1.42 ± 0.07	0.9870
617	1.36 ± 0.07	0.9858
622	1.31 ± 0.07	0.9847
627	1.27 ± 0.07	0.9844
632	1.24 ± 0.07	0.9855
637	1.23 ± 0.06	0.9884
642	1.35 ± 0.06	0.9924
647	1.33 ± 0.06	0.9921
652	1.31 ± 0.06	0.9915
657	1.40 ± 0.08	0.9888
662	1.42 ± 0.09	0.9888

Fig. 10 XRD pattern of frit A4 subjected to thermal treatment for crystallization

Fig. 11 Optical micrograph of the aventurine crystallized glaze ×400

Fig. 12 Optical micrograph of the aventurine crystallized glaze ×1000

The hematite crystallization degree and the crystals shape and size were analyzed by optical microscopy in reflected light (Figs. 11, 12).

The image in Fig. 12 clearly reveals the presence of hexagonal hematite crystals disposed relatively uniform in the vitreous matrix.

According to the literature data [26–30], this value could be interpreted in terms of overlapping of surface crystallization ($n = 1.0$) and one-dimensional growth ($n = 2.0$).

The hematite crystallization in the studied aventurine glaze was confirmed by XRD analysis. Figure 10 shows the XRD pattern of frit A4 after thermal treatment at 800 °C followed by slow cooling with 30 min soaking time, at 630 °C.

One may notice that hematite is the single crystalline phase presents in the sample, embedded in the glassy matrix, indicated by the high background at 2(angles between 22° and 30°.

Conclusions

- The apparent activation energy of the hematite crystallization in the studied aventurine glaze ranges with the crystallized fraction between 150 and 180 kJ mol^{-1}.
- The activation energies evaluated by KAS, Starink, Tang, and Vyazovkin methods show very close values in the entire range of the crystallized fraction and a little lower compared with the activation energies evaluated by OFW method.
- The activation energy varies with the crystallized fraction regardless of the method used confirming the complex mechanism of the hematite crystallization process in the aventurine glaze.

- The Avrami exponent values, calculated by Ozawa method, also confirm the complex mechanism of the crystallization process.

References

1. Dakhai S, Orlova LA, Mikhailenko NYu. Types and compositions of crystalline glazes (a review). Glass Ceram. 1999;58: 177–80.
2. Levitskii IA. Mechanism of phase formation in aventurine glaze. Glass Ceramics. 2001;58:223–6.
3. Dvornichenko IN, Matsenko SV. Production of iron-containing crystalline glazes. Glass Ceramics. 2000;57:67–8.
4. Vyazovkin S, Wight CA. Model-free and model-fitting approaches to kinetic analysis of isothermal and non-isothermal data. Thermochim Acta. 1999;340–341:53–68.
5. Starink MJ. The determination of activation energy from linear heating rate experiments: a comparison of the accuracy of iso-conversion methods. Thermochim Acta. 2003;404:163–76.
6. Khawam A, Flanagan DR. Role of isoconversional methods in varying activation energies of solid-state kinetics II. Non-isothermal kinetic studies. Thermochim Acta. 2005;436:101–12.
7. Starink MJ. Activation energy determination for linear heating rate experiments: deviations due to neglecting the low temperature end of the temperature integral. J Mater Sci. 2007;42:483–9.
8. Criado JM, Sanchez-Jimenez PE, Perez-Maqueda LA. Critical study of the isoconversional methods of kinetic analysis. J Therm Anal Calorim. 2008;92:199–203.
9. Cai JM, Liu RH. Precision of integral methods for the determination of the kinetic parameters. J Therm Anal Calorim. 2008;91(1): 275–8.
10. Sbirrazzuoli N, Vincent L, Bouillard J, Elegant L. Isothermal and non-isothermal kinetics when mechanistic information available. J Therm Anal Calorim. 1999;56:783–92.
11. Cai JM, Liu RH. Non-isothermal kinetics in solids. The precision of some integral methods for the determination of the activation energy without neglecting the temperature integral at the starting temperature. J Therm Anal Calorim. 2008;94:313–6.
12. Vyazovkin S. A unified approach to kinetic processing of non-isothermal data. Int J Chem Kinet. 1996;28:95–101.
13. Vyazovkin S, Dollimore D. Linear and nonlinear procedures in isoconversional computations of the activation-energy of non-isothermal reactions in solids. J Chem Inf Comp Sci. 1996;36: 42–5.
14. Pratap A, Rao TLS, Lad KN, Dhurandhar HD. Isoconversional vs model fitting methods. A case study of crystallization kinetics of a Fe-based metallic glass. J Therm Anal Calorim. 2007;89(2):399–405.
15. Chen HX, Liu NA. Approximations for the temperature integral: their underlying relationship. J Therm Anal Calorim. 2008;92(2): 573–8.
16. Burnham AK, Dinh LN. A comparison of isoconversional and model-fiting approaches to kinetic parameter estimation and application predictions. J Therm Anal Calorim. 2007;89(2): 479–90.
17. Doyle CD. Series approximations to the equation of thermo-gravimetric data. Nature. 1965;207:290–1.
18. Wanjun T, Yuwen L, Hen Z, Cunxin W. New approximate formula for Arrhenius temperature integral. Thermochim Acta. 2003; 408:39–43.
19. Wanjun T, Donghua C. An integral method to determine variation in activation energy with extent of conversion. Thermochim Acta. 2005;433:72–6.
20. Vyazovkin S. Advanced isoconversional method. J Therm Anal Calorim. 1997;49:1493–9.
21. Vyazovkin S, Dranca I. Isoconversional analysis of combined melt and glass crystallization data. Macromol Chem Phys. 2006; 207:20–5.
22. Wanjun T, Yuwen L, Hen Z, Zhiyong W, Cunxin W. New temperature integral approximate formula for non-isothermal kinetic analysis. J Therm Anal Calorim. 2003;74:309–15.
23. Saha B, Maiti AK, Ghoshal AK. Model-free method for iso-thermal and non-isothermal decomposition kinetics analysis of PET sample. Thermochim Acta. 2006;444:46–52.
24. Saha B, Ghoshal AK. Model-free kinetics analysis of waste PE sample. Thermochim Acta. 2006;451:27–33.
25. Ozawa T. Kinetics of non-isothermal crystallization. Polymer. 1971;12:150–8.
26. Matusita K, Sakka S. Kinetic study of crystallization of glass by differential thermal analysis-criterion on application of Kissinger plot. J Non-Cryst Solids. 1980;38–39:741–6.
27. Afify N, Abde-Rahim MA, Abd El-Halim AS, Hafiz MM. Kinetics study of non-isothermal crystallization in $Se_{0.7}Ge_{0.2}Sb_{0.1}$ chalcogenide glass. J Non-Cryst Solids. 1991;128:269–78.
28. Tomasi C, Scavini M, Speghini A, Bettinelli M, Riccardi MP. Devitrification kinetics of $PbGeO_3$ Isothermal and non-isothermal study. J Therm Anal Calorim. 2002;70:151–64.
29. Iordanova R, Lefterova E, Uzunov I, Dimitriev Y, Klissurski D. Non-isothermal crystallization kinetics of V_2O_5-MoO_3-Bi_2O_3 glasses. J Therm Anal Calorim. 2002;70:393–404.
30. Mehta N, Agarwal P, Kumar A. A study of the crystallization kinetics in $Se_{68}Ge_{22}Pb_{10}$ chalcogenide glass. Indian J Eng Mater Sci. 2004;11:511–5.